

Exact Spectral Analysis of Traditional and Single-Source Integral Equations for a Penetrable Sphere

Martijn Huynen, Dries Vande Ginste, and Vladimir Okhmatovski



Quantum
Mechanical &
Electromagnetic
Systems
Modelling Lab

quest.



imec



University
of **Manitoba**

Boundary integral equations

Upsides and downsides

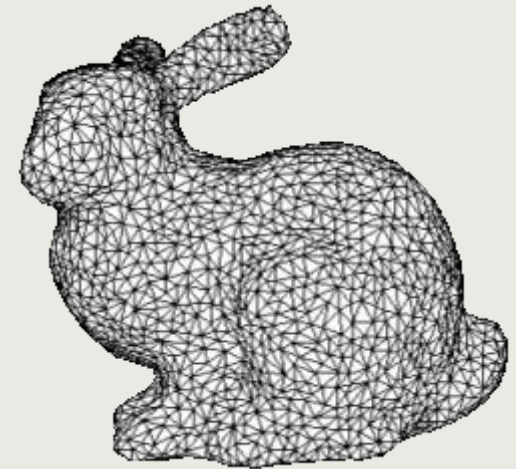
Boundary integral equations (BIEs) are characterized by their use of the Green's function and restriction of the unknowns to the boundary

This results in a **smaller system matrix** and automatic **inclusion** of the **radiation condition**

but also in a **dense matrix** with more **difficult** numerical **calculation**, especially for **good** conductors

Moreover, BIEs are known to suffer from low-frequency breakdown, dense-mesh breakdown, internal resonances etc.

As these properties often depend on the discretization strategy, inherent analysis of the BIE's properties is difficult



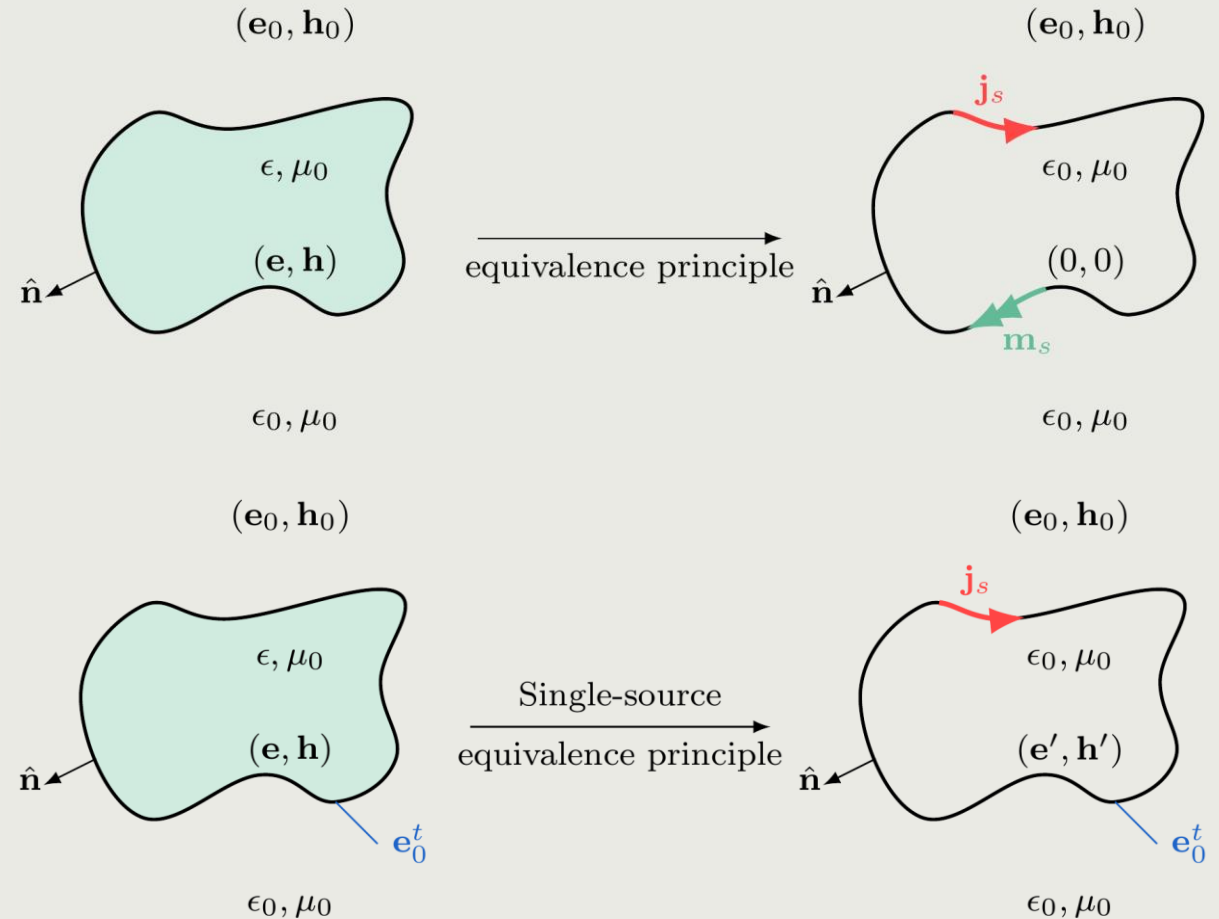
Boundary integral equations

Equivalence theorem

Central to all BIEs is the equivalence theorem, which typically introduces **two** boundary sources \mathbf{j}_s and \mathbf{m}_s to replace the material inside leading to formulation such as the PMCHWT and Müller BIE

However, by giving up control over the fields inside, a **single-source** suffices leading to formulations such as the Surface-Volume-Surface-EFIE (SVS-EFIE) & the Differential Surface Admittance-EFIE (DSA-EFIE)

Single-source formulations typically studied less in-depth



Boundary integral equations

Differential surface admittance operator

DSA approach has been successfully applied to various problem such as

- 2-D transmission Line RLGC extraction [1]
- Arbitrary interconnect characterization [2]
- 3-D scattering & interconnects of canonical volumes [3]
- Development of magnetic interconnects [4]

However, rigorous **proof** of the DSA's rigor, inherent properties & weaknesses, and the effects of magnetic contrast is still lacking

Goal: derive **analytical solution** for a sphere, compute **closed-form eigenvalues** and study effect **breakdown** on condition number

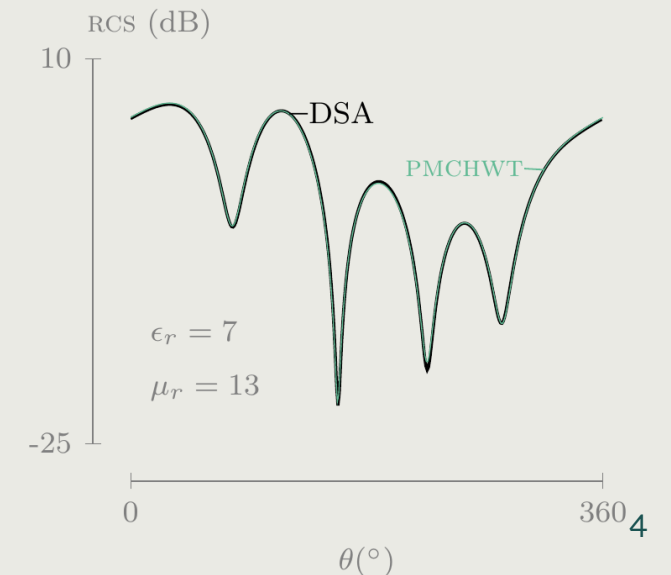
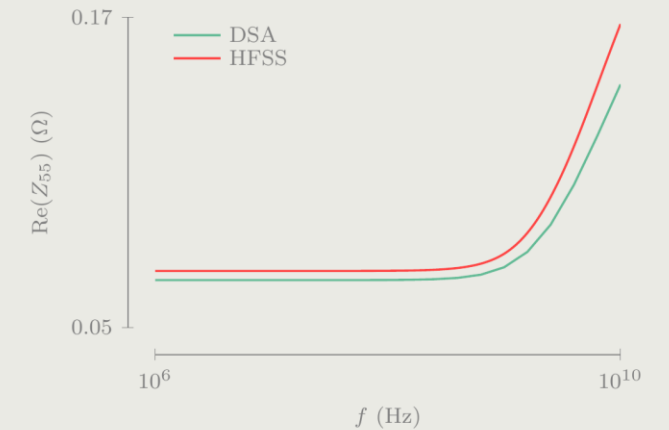
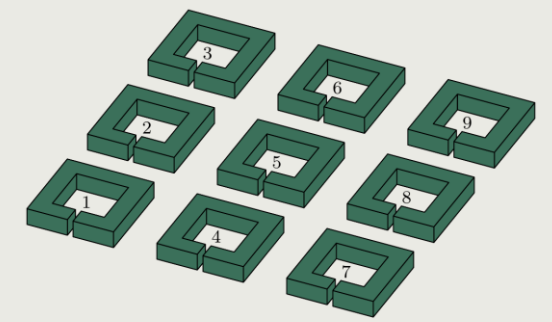


[1] Demeester, IEEE MTT 2008

[2] Patel, IEEE MTT 2016

[3] Huynen, IEEE MTT 2020

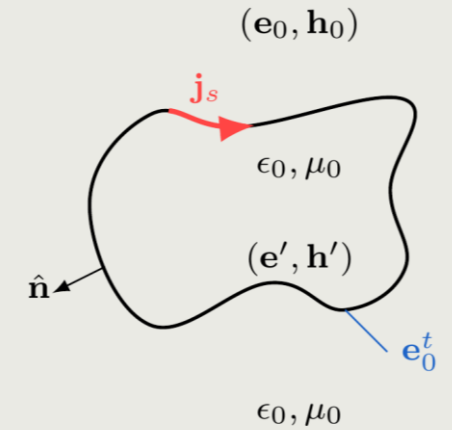
[4] Bosman, IEEE MTT 2023



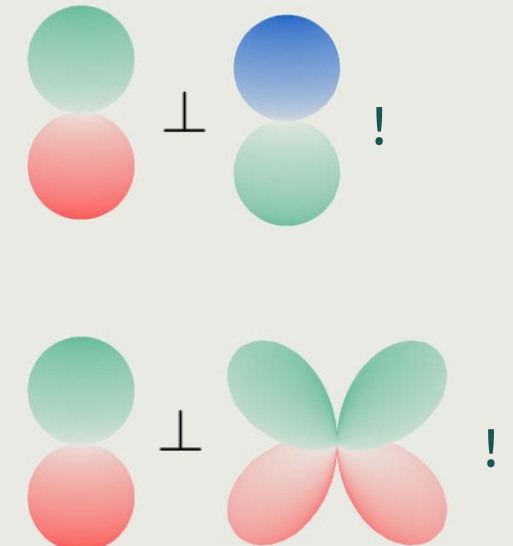
Spherical harmonics-based decomposition

Boundary quantities

The surface current density \mathbf{j}_s and tangential electric field \mathbf{e}_0^t are decomposed into **two** sets of vector spherical harmonics



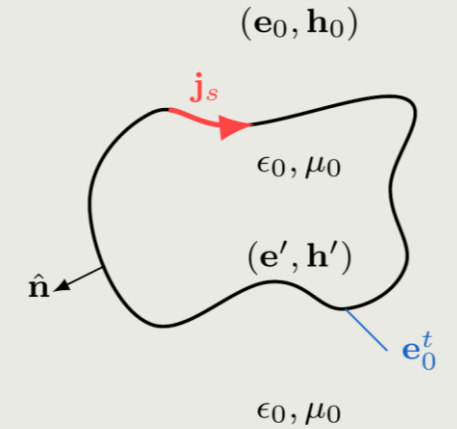
$$\begin{aligned}
 \mathbf{j}_s = & \alpha_{10}^{(1)} \begin{array}{c} \text{Green circle} \\ \text{Red circle} \end{array} + \alpha_{20}^{(1)} \begin{array}{c} \text{Green lobe} \\ \text{Red lobe} \end{array} + \alpha_{21}^{(1)} \begin{array}{c} \text{Green lobe} \\ \text{Red lobe} \end{array} + \dots \\
 & + \alpha_{10}^{(2)} \begin{array}{c} \text{Blue circle} \\ \text{Green circle} \end{array} + \alpha_{20}^{(2)} \begin{array}{c} \text{Blue lobe} \\ \text{Green lobe} \end{array} + \alpha_{21}^{(2)} \begin{array}{c} \text{Blue lobe} \\ \text{Green lobe} \end{array} + \dots \\
 \mathbf{e}_0^t = & \beta_{10}^{(1)} \begin{array}{c} \text{Green circle} \\ \text{Red circle} \end{array} + \beta_{20}^{(1)} \begin{array}{c} \text{Green lobe} \\ \text{Red lobe} \end{array} + \beta_{21}^{(1)} \begin{array}{c} \text{Green lobe} \\ \text{Red lobe} \end{array} + \dots \\
 & + \beta_{10}^{(2)} \begin{array}{c} \text{Blue circle} \\ \text{Green circle} \end{array} + \beta_{20}^{(2)} \begin{array}{c} \text{Blue lobe} \\ \text{Green lobe} \end{array} + \beta_{21}^{(2)} \begin{array}{c} \text{Blue lobe} \\ \text{Green lobe} \end{array} + \dots
 \end{aligned}$$



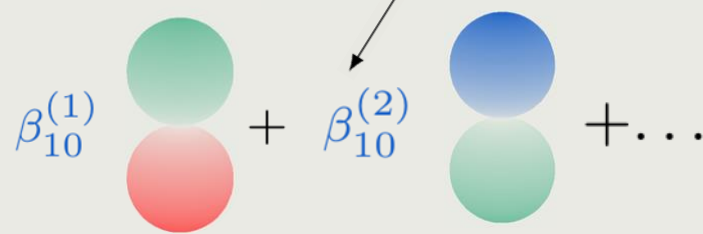
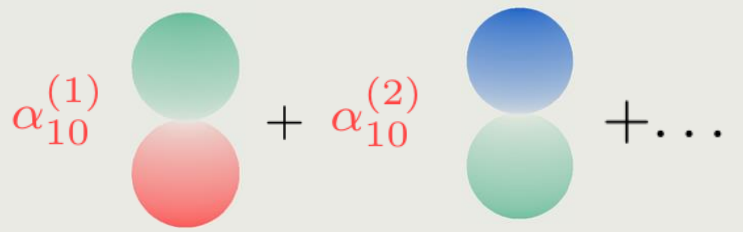
Spherical harmonics-based decomposition

Electric Field Integral Equation (EFIE)

In the EFIE, the Green's kernel can be expanded into  and  well



$$\hat{\mathbf{n}} \times \mathbf{e}_0^t(\mathbf{r}) = \hat{\mathbf{n}} \times \mathbf{e}_{\text{inc}} - j\omega\mu_0 \hat{\mathbf{n}} \times \int_S \overline{\overline{\mathbf{G}}_0(|\mathbf{r} - \mathbf{r}'|)} \mathbf{j}_s(\mathbf{r}') d\mathbf{r}'$$

which, after Galerkin testing, leads to a one-to-one correspondence between every $\alpha_n^{(1)}$ and $\beta_n^{(1)}$, and every $\alpha_n^{(2)}$ and $\beta_n^{(2)}$

$$\beta_{nm}^{(1)} = \gamma_{nm} + \mathcal{Z}_n^{(1)} \alpha_{nm}^{(1)}$$

$$\beta_{nm}^{(2)} = \gamma_{nm} + \mathcal{Z}_n^{(2)} \alpha_{nm}^{(2)}$$



$$\mathcal{Z}_n^{(1)} \propto [k_0 a j_n(k_0 a)]' [k_0 a h_n^{(2)}(k_0 a)]'$$

$$\mathcal{Z}_n^{(2)} \propto k_0 a j_n(k_0 a) k_0 a h_n^{(2)}(k_0 a)$$

Spherical harmonics-based decomposition

Differential surface admittance operator (DSA)

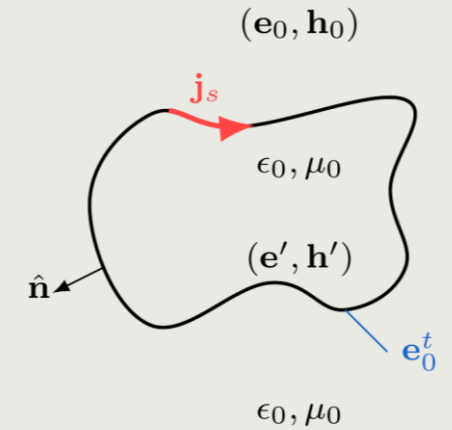
The DSA operator can be constructed in various ways to find the electric surface current density \mathbf{j}_s [5], [6]

The original formulation and its 3-D extension rely on the eigenmodes of a PEC cavity and avoid the Green's function in the medium

For a sphere, the two groups of eigenmodes are of the form:

$$\mathbf{h}_{nms}^{\text{TM}} \propto j_n(k_{ns}r) \begin{array}{c} \text{blue lobe} \\ \text{green lobe} \end{array}$$

$$\mathbf{h}_{nms}^{\text{TE}} \propto j_n(k_{ns}r) \begin{array}{c} \text{green lobe} \\ \text{red lobe} \end{array}$$



Spherical harmonics-based decomposition

Differential surface admittance operator (DSA)

With these spherical harmonics form of the eigenmodes, we discretize

$$\mathbf{j}_s(\mathbf{r}) = -\eta \sum_{nms} \left[\frac{\mathcal{K}_{nms}}{\mathcal{N}_{nms}^2} \int_S (\hat{\mathbf{n}} \times \mathbf{h}_{nms}^*(\mathbf{r}')) \cdot \mathbf{e}_0^t(\mathbf{r}') d\mathbf{r}' \right] (\hat{\mathbf{n}} \times \mathbf{h}_{nms}(\mathbf{r}))$$

which, after Galerkin testing, leads to a one-to-one correspondence between every $\alpha_n^{(1)}$ and $\beta_n^{(1)}$, and every $\alpha_n^{(2)}$ and $\beta_n^{(2)}$

$$\alpha_n^{(1)} = \mathcal{Y}_n^{(1)} \beta_n^{(1)}$$

$$\alpha_n^{(2)} = \mathcal{Y}_n^{(2)} \beta_n^{(2)}$$

$$\mathcal{Y}_n^{(1)} \propto \sum_s \frac{-2k_{ns}^2 (k^2 - k_0^2)}{(k_{ns}^2 - k^2) (k_{ns}^2 - k_0^2) \left[1 - \frac{n(n+1)}{k_{ns}^2} \right]}$$

$$\mathcal{Y}_n^{(2)} \propto \sum_s \frac{-2\kappa_{ns}^2 (k^2 - k_0^2)}{(\kappa_{ns}^2 - k^2) (\kappa_{ns}^2 - k_0^2)}$$



Spherical harmonics-based decomposition

Analytical solution

With both operators discretized and resulting in simple one-to-one relations, the system is easily solved:

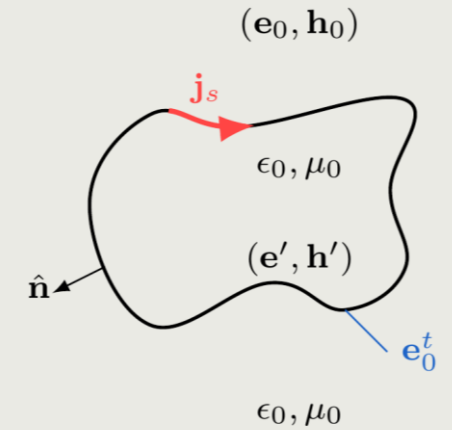
$$\beta_{nm}^{(1)} = \gamma_{nm} / (1 - \mathcal{Z}_n^{(1)} \mathcal{Y}_n^{(1)}) \quad \alpha_{nm}^{(1)} = \mathcal{Y}_n^{(1)} \gamma_{nm} / (1 - \mathcal{Z}_n^{(1)} \mathcal{Y}_n^{(1)})$$

$$\beta_{nm}^{(2)} = \gamma_{nm} / (1 - \mathcal{Z}_n^{(2)} \mathcal{Y}_n^{(2)}) \quad \alpha_{nm}^{(2)} = \mathcal{Y}_n^{(2)} \gamma_{nm} / (1 - \mathcal{Z}_n^{(2)} \mathcal{Y}_n^{(2)})$$

Since the solution is fully analytical, it should be rigorous compared to the exact solution

However, the DSA elements contain an infinite sum

- Convergence rate?
- Effect different materials?
- Does it jeopardize the DSA's exactness?



Closed-form DSA elements

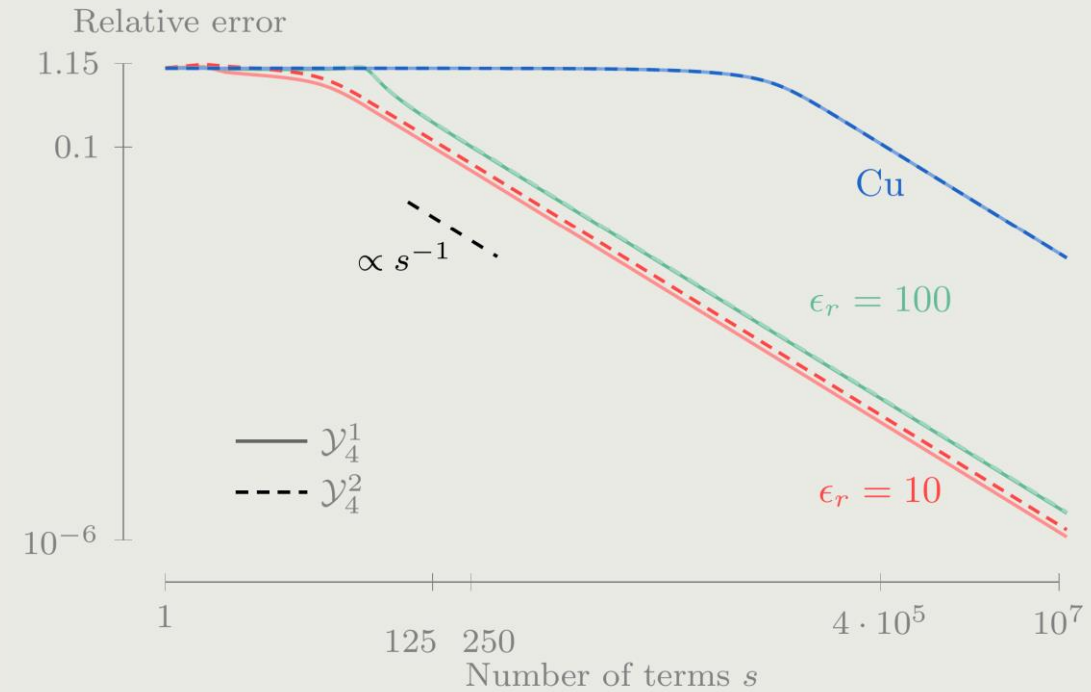
Analytical solution

The sums require the **zeros** of the **Bessel functions**, which need to be computed **numerically**

The sums only converge at a **rate s^{-1}** , which is slow if machine precision is desirable

For **high-contrast** materials or **good conductors** a very slow initial convergence is observed

Solution: closed-form expression based on generalized Fourier series



Closed-form DSA elements

Analytical solution

Just like for the conventional Fourier series, the function \mathbf{f} is projected on a set of orthogonal basis functions

$$\mathbf{f}(\mathbf{r}) \sim \sum_{s=0}^{\infty} \frac{\langle \mathbf{f}, j_n(k_{ns}\mathbf{r}) \rangle}{\|j_n(k_{ns}\mathbf{r})\|^2} j_n(k_{ns}\mathbf{r})$$

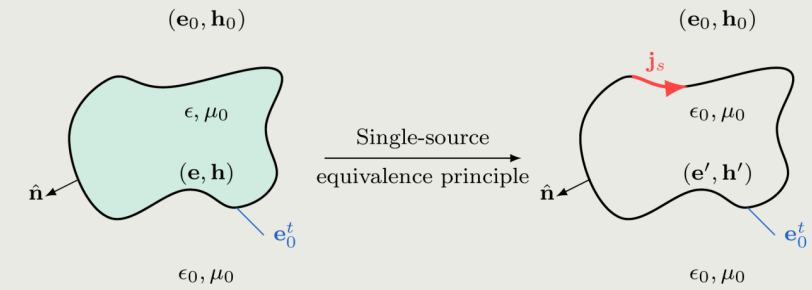
By choosing the correct \mathbf{f} , the Fourier sum becomes $\mathcal{Y}_n^{(1)}$ and $\mathcal{Y}_n^{(2)}$

hence their closed form is found to be

$$\mathcal{Y}_n^{(1)} \propto \frac{(ka)^2 j_n(ka)}{[kaj_n(ka)]'} - \frac{(k_0a)^2 j_n(k_0a)}{[k_0aj_n(k_0a)]'}$$

$$\mathcal{Y}_n^{(2)} \propto ka \frac{[kaj_n(ka)]'}{j_n(ka)} - k_0a \frac{[k_0aj_n(k_0a)]'}{j_n(k_0a)}$$

Leading to **fast, accurate** evaluations for the final solution



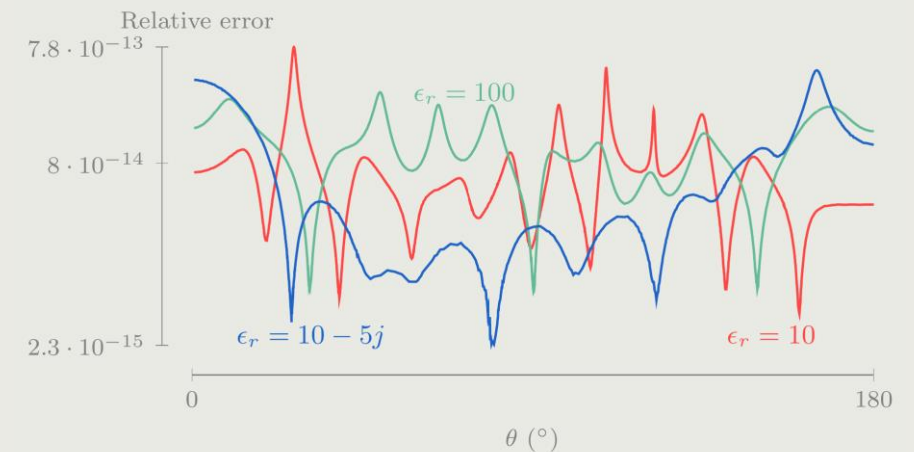
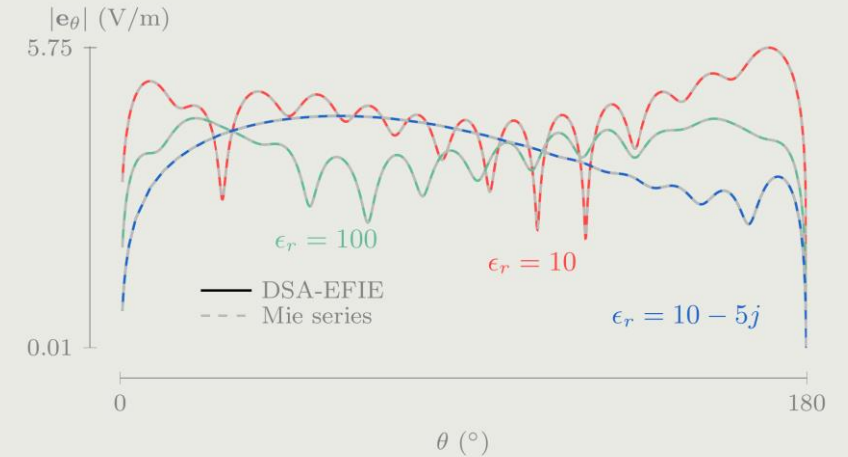
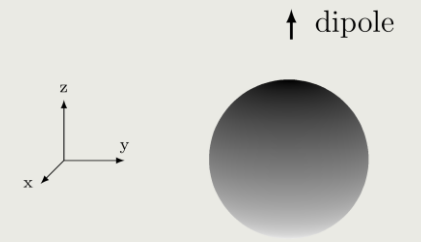
Numerical results

Radial dipole

Parameters set-up

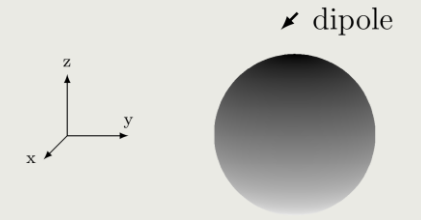
- Radius sphere: 1 m
- Distance dipole from origin: 10 m
- Dipole moment: 1 A m
- Frequency: $k_0 = 4\pi / 1\text{m}$
- # terms in Mie series: 50
- # terms in DSA-EFIE: 50
- 3 different materials:
 - Low-contrast dielectric
 - High-contrast dielectric
 - Lossy dielectric

> 12 significant digits compared to the Mie series
so the DSA-EFIE provides a rigorous solution



Numerical results

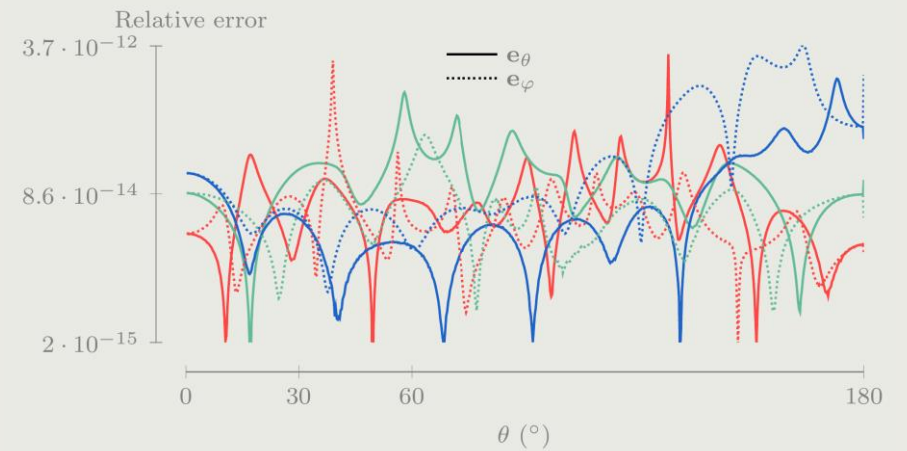
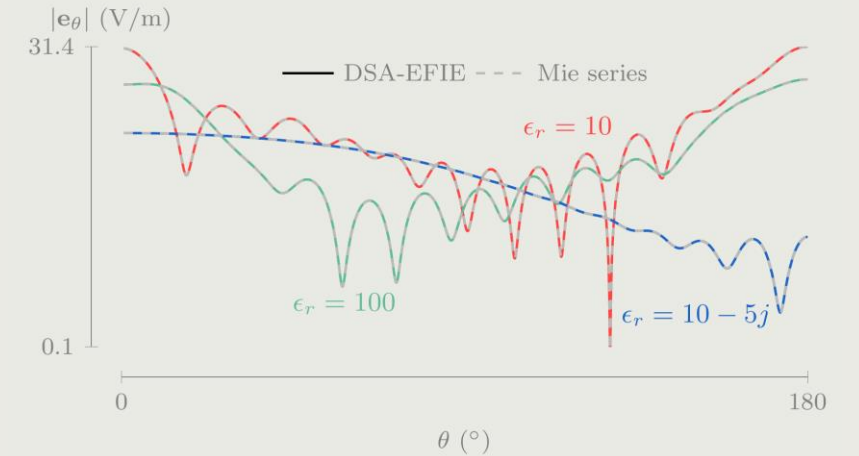
Tangential dipole



Parameters set-up

- Radius sphere: 1 m
- Distance dipole from origin: 10 m
- Dipole moment: 1 A m
- Frequency: $k_0 = 4\pi / 1\text{m}$
- # terms in Mie series: 50
- # terms in DSA-EFIE: 50
- 3 different materials:
 - Low-contrast dielectric
 - High-contrast dielectric
 - Lossy dielectric

> 12 significant digits compared to the Mie series
so the DSA-EFIE provides a rigorous solution



Numerical results

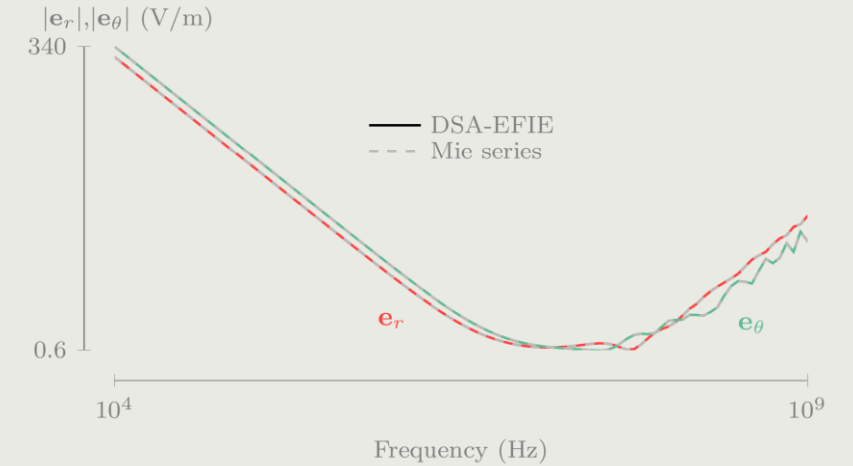
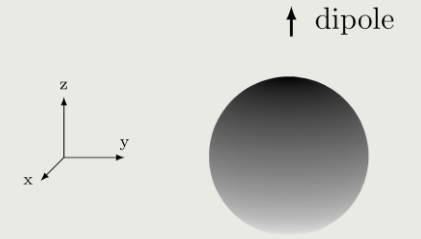
Radial dipole, good conductor

Parameters set-up

- Radius sphere: 1 m
- Distance dipole from origin: 10 m
- Dipole moment: 1 A m
- Frequency: $k_0 = 4\pi / 1\text{m}$
- # terms in Mie series: 50
- # terms in DSA-EFIE: 50
- Copper ($\sigma=5,8\text{e}7 \text{ S/m}$) from 10 kHz up to 1 GHz
- Observation point at 1 m above the surface for $\theta = \pi/4$

> 15 significant digits compared to the Mie series

so the DSA-EFIE provides a rigorous solution for this difficult-to-handle class of materials



Spectral analysis

Dense-mesh breakdown

$\mathcal{Z}_n^{(1)} \mathcal{Y}_n^{(1)}$ and $\mathcal{Z}_n^{(2)} \mathcal{Y}_n^{(2)}$ are the eigenvalues of the DSA-EFIE system

For large n , one set of eigenvalues accumulates at zero, while the other stays constant

this leads to **dense-mesh breakdown**

Choice of Sobolev space does not solve the issue

Comparison:

- EFIE [7] : Sobolev $H^{-1/2}$ (div) testing avoids dense-mesh breakdown
- MFIE [7] : L^2 testing avoids dense-mesh breakdown
- SVS-EFIE-J [8]: Sobolev $H^{-1/2}$ (div) testing avoids dense-mesh breakdown
- SVS-EFIE-M [9]: L^2 testing avoids dense-mesh breakdown



Spectral analysis

Low-frequency breakdown

$\mathcal{Z}_n^{(1)} \mathcal{Y}_n^{(1)}$ and $\mathcal{Z}_n^{(2)} \mathcal{Y}_n^{(2)}$ are the eigenvalues of the DSA-EFIE system

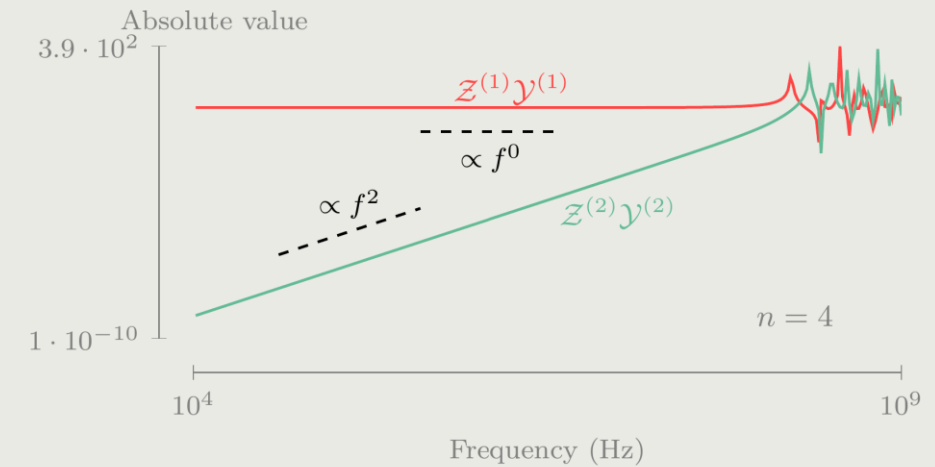
For small f , one set of eigenvalues accumulates at zero, while the other stays constant

this leads to **low-frequency breakdown**

Inherent to the EFIE so Sobolev testing space does not solve this issue

Comparison:

- EFIE [7] : Inherent low-frequency breakdown
- MFIE [7] : Absence of low-frequency breakdown
- SVS-EFIE-J [8]: Inherent low-frequency breakdown
- SVS-EFIE-M [9]: Absence of low-frequency breakdown



Conclusion

& future work

We presented an **analytic solution** to the **Differential Surface Admittance operator** combined with the **EFIE** for scattering at a **sphere**

Analytical solution is **devoid** of any remaining **summation** or **numerical integration** and provides **>12 significant digits**

Spectral analysis confirms **dense-mesh breakdown** and **low-frequency breakdown**

Developed exact **solution** is an excellent **analytical tool** to develop **new DSA-BIE formulations** with preferable properties



quest. Quantum Mechanical &
Electromagnetic Systems
Modelling Lab

Technologiepark – Zwijnaarde 126, B-9052 Gent, Belgium
Martijn.huynen@ugent.be
www.QuestLab.be

Martijn HUYNEN, Post-doctoral researcher

